Detailed β-transition rates for URCA nuclear pairs in 8–10 solar-mass stars

Hiroshi Toki,[1,*] Toshio Suzuki,[2,†] Ken'ichi Nomoto,[3,‡] Samuel Jones,[4] and Raphael Hirschi[4,3]
[1]*Research Center for Nuclear Physics (RCNP), Osaka University, Ibaraki, Osaka 567-0047, Japan*
[2]*Department of Physics, College of Humanities and Sciences, Nihon University, Setagaya-ku, Tokyo 156-8550, Japan*
[3]*Kavli Institute for the Physics and Mathematics of the Universe (WPI), The University of Tokyo, Kashiwa, Chiba 277-8583, Japan*
[4]*Astrophysics Group, Lennard Jones Building, Keele University, Staffordshire ST5 5BG, United Kingdom*
(Received 29 May 2013; revised manuscript received 23 June 2013; published 15 July 2013)

We calculate β-transition rates for URCA nuclear pairs using the sd-shell-model framework of Wildenthal [B. H. Widenthal, Prog. Part. Nucl. Phys. **11**, 5 (1984)] with the modified Hamiltonian. We consider many β transitions including excited states necessary for electron capture and β decay with high Fermi energy of electrons at high electron density ρY_e and temperature T relevant for the massive star and super-asymptotic-giant-branch star evolution. We provide β-transition rates for URCA nuclear pairs ($A = 23$, 25, and 27) in the range of density $8.0 < \log_{10} \rho Y_e < 9.2$ in steps of 0.02 (Y_e is the electron mole number and ρ is the nucleon density in units of g cm^{-3}) and temperature $8.0 < \log_{10} T < 9.2$ in steps of 0.05 (T is the temperature in units of K). This fine mesh is able to provide clearly the URCA density at $\log_{10} \rho Y_e = 8.92$ for $A = 23$ and at $\log_{10} \rho Y_e = 8.81$ for $A = 25$, while the URCA density is not clear for $A = 27$. For the evolution of 8–10$M_\odot$ stars, the use of the fine mesh is found to increase the cooling effect and affects the final fate of these stars.

DOI: 10.1103/PhysRevC.88.015806 PACS number(s): 21.60.Cs, 23.40.−s, 27.30.+t

I. INTRODUCTION

Stars of the mass above $0.5M_\odot$ and below $8M_\odot$ burn helium and develop electron-degenerate cores consisting of carbon and oxygen (C-O). The final fate of these stars is the formation of C-O white dwarfs. Stars more massive than $8M_\odot$ are able to burn carbon to form oxygen-neon-magnesium (O-Ne-Mg) cores. Stars above $10M_\odot$ reach the Fe core and have a fate of core collapse supernova explosion. However, it is not certain at present whether the final fate of 8–10$M_\odot$ stars is the formation of an O-Ne-Mg white dwarf, the collapse of an O-Ne-Mg core, or the collapse of an Fe core (for a review, see, e.g., Nomoto and Hashimoto [1]). Among other uncertainties, this is due to the lack of detailed input of nuclear β-transition rates.

As the O-Ne-Mg core of 8–10$M_\odot$ stars evolve, the matter density and temperature in the central region increase and the Fermi energy of electrons reaches the threshold energy of electron capture on various nuclei produced by nuclear reactions in stars. The electron-capture process has two competitive effects. Because stars are supported by the pressure of degenerate electrons, the decrease of electrons facilitates the collapse of the core. Second, the entropy production associated with the electron capture increases the temperature and induces explosive oxygen burning. The final fate of the O-Ne-Mg core strongly depends on the effects of electron capture [2–4].

Hence, there are many studies to provide β-transition rates using ft values calculated by the shell model for sd-shell nuclei. These β-transition processes compete in these massive stars and the fates of these stars depend on the β-transition rates of nuclei in the mass range of $16 < A < 40$. These nuclei are called sd-shell nuclei because the valence orbits of protons and neutrons of these nuclei are 1s and 0d shell orbits.

In the electron-capture process of sd-shell nuclei, there is a very interesting cooling mechanism, which is called the nuclear URCA process. The electron capture favors high density so that the Fermi energy of electrons exceeds the threshold energy, while the β-decay favors low density because the electron Fermi surface blocks the phase space of the decaying electrons. Hence, for a particular nuclear pair, a condition may be fulfilled where both the electron capture and the β decay happen simultaneously. In this case, nuclear abundances and even the Fermi sea do not change, but the produced neutrinos and antineutrinos escape from the stellar interior. This nuclear URCA process is an effective mechanism to cool down the O-Ne-Mg core of stars. The nuclear URCA pairs of interest for the evolution of 8–10$M_\odot$ stars are

(i) $A = 23$: $^{23}\mathrm{Na} + \mathrm{e}^- \rightarrow {}^{23}\mathrm{Ne} + \nu$ and $^{23}\mathrm{Ne} \rightarrow {}^{23}\mathrm{Na} + \mathrm{e}^- + \bar{\nu}$,
(ii) $A = 25$: $^{25}\mathrm{Mg} + \mathrm{e}^- \rightarrow {}^{25}\mathrm{Na} + \nu$ and $^{25}\mathrm{Na} \rightarrow {}^{25}\mathrm{Mg} + \mathrm{e}^- + \bar{\nu}$, and
(iii) $A = 27$: $^{27}\mathrm{Al} + \mathrm{e}^- \rightarrow {}^{27}\mathrm{Mg} + \nu$ and $^{27}\mathrm{Mg} \rightarrow {}^{27}\mathrm{Al} + \mathrm{e}^- + \bar{\nu}$.

These nuclei belong to the sd-shell region. Due to many experimental data on energy spectra and γ transitions with theoretical efforts to describe these data using the shell model, we have an extremely useful shell model to reproduce the energy spectra and γ transitions [5,6]. This fact allows us to calculate all the necessary information for the calculation of all the β-transition rates. In fact, there are preceding works on β-transition rates for the sd-shell nuclei [7–10]. All these theoretical works include β transitions of excited states, which could be provided only by the shell model. Because these studies are planned to provide β-transition rates to be used for a wide range of applications, the most frequently used table of Oda *et al.* [10] is obtained at sparse temperature and density spaces. For the usual stellar evolution calculations Oda *et al.*'s table may be fine, but for sensitive processes such as the URCA

*toki@rcnp.osaka-u.ac.jp
†suzuki@phys.chs.nihon-u.ac.jp
‡nomoto@astron.s.u-tokyo.ac.jp

 ©2013 American Physical Society

nuclear process in the evolution of intermediate mass stars this sparse mesh table is not good enough.

Hence, in this paper we want to study β-transition rates of the URCA nuclear pairs for careful stellar evolution calculations using the sd-shell model. We use the sd-shell model of Wildenthal [5] for the excitation energies and the ft values of the URCA nuclear pairs. In Sec. II, we briefly describe the sd-shell model and write the method of calculation of the β-transition rates, the neutrino-energy-loss rates, and the γ-heating rates. In Sec. III, we provide the reaction rates focusing on the URCA nuclear process. In Sec. IV, we discuss the Coulomb correction effect on β-transition rates due to the electron wave function around the nucleus. In Sec. V, we present one example of stellar evolution calculations to discuss the URCA processes with the use of the new table. Section VI is devoted to a summary of the present work.

II. SHELL MODEL FOR sd-SHELL NUCLEI AND β TRANSITIONS

We describe briefly the shell model for sd-shell nuclei and calculations of β-transition ft values and β-transition rates. The construction of the shell-model wave functions for sd-shell nuclei is described by Brown and Wildenthal [5,6]. In the shell model, $0s$ and $0p$ shells are completely occupied by nucleons (16 nucleons) and remaining nucleons occupy $1s$ and $0d$ shells. These nucleons are described by all the possible sd-shell-model configurations. The effective model Hamiltonian for these calculations was determined empirically, where 63 two-body matrix elements and 3 single-particle energies were treated as free parameters. They were fixed by making least-squares fits of shell-model eigenvalues to experimental excitation energies. The wave functions obtained by diagonalizing this Hamiltonian could then be used to calculate various observables. Comparisons of such predictions with experiment have confirmed the overall validity of these wave functions and the predictions for other observables can be considered "semiempirical." The work on Gamow-Teller (GT) β-transitions is particularly relevant for the present study. All the known β-decay ft values have been compared with the shell-model predictions [11]. The shell-model Hamiltonian was modified in 2006 by using an updated set of binding energies and energy levels [12]. We use the Hamiltonian USDB in this work [12].

The ft value is written as

$$ft = \frac{6147}{B(F) + (g_A/g_V)^2 B(\mathrm{GT})}. \tag{1}$$

Here, $B(F)$ is the reduced transition probability of the Fermi transition and $B(\mathrm{GT})$ is that of the Gamow-Teller transition. The ratio $g_A/g_V = 1.263$ denotes the nucleon weak axial-vector and vector transition coupling constants. They are given by the nuclear matrix elements between the i and j states:

$$\begin{aligned} B(F)_{ij} &= \left| \langle j || \sum_k t_+^k || i \rangle \right|^2 / (2I_i + 1), \\ B(\mathrm{GT})_{ij} &= \left| \langle j || \sum_k \sigma^k t_+^k || i \rangle \right|^2 / (2I_i + 1). \end{aligned} \tag{2}$$

Here, I_i denotes the total spin of the initial state, σ_k the Pauli spin matrix, and $t_\pm$ the isospin operator. The GT matrix elements require detailed initial- and final-state wave functions. They are provided by the sd-shell model calculations and with the quenching factor of $(qf)^2 = 0.764^2$ the GT transitions reproduce available experimental data [12].

The β-transition rates λ_{ij} for a particular transition between i and j nuclear states are obtained by using the ft values and kinematical quantities f_{ij} to take care of electron distributions around the nucleus at various temperatures T and electron densities ρ_e:

$$\lambda_{ij} = \frac{f_{ij}(T, \rho_e, U_F)}{(ft)_{ij}} \ln 2. \tag{3}$$

We write the electron density as $\rho_e = \rho Y_e$, where ρ is the nucleon density and Y_e is the electron mole number. The chemical potential of electrons is denoted by U_F. The kinematical quantities f_{ij} are written in detail in the paper of Fuller *et al.* [7]. These β-transition rates are used for various quantities together with the occupation probability P_i of the ith state due to thermal equilibrium,

$$P_i = \frac{(2I_i + 1)\exp(-E_i/kT)}{\sum_j (2I_j + 1)\exp(-E_j/kT)}. \tag{4}$$

Here, E_i is the excitation energy of ith state and k is the Boltzmann constant. The β-transition rate for parent-to-daughter nuclei is

$$\lambda = \sum_{ij} P_i \lambda_{ij}. \tag{5}$$

The neutrino-emission rate associated with the β transition is

$$\lambda(\nu) = \sum_{ij} P_i \lambda_{ij}^{\nu}, \tag{6}$$

where λ_{ij}^{ν} is obtained in the kinematical integrations f_{ij} by weighting the neutrino energies. The heating rate associated with the β transition is

$$\lambda(\gamma) = \sum_{ij} P_i \lambda_{ij} E_j. \tag{7}$$

In the heating rate due to γ transitions, we assume that all the excitation energies in the daughter nucleus are used for direct and/or multiple γ transitions to the ground state.

For the calculation of β-transition rates of the URCA nuclear pairs in the density and temperature ranges of interest, we should include excited states of the initial and final states. For electron-capture reactions, all the initial states with excitation energy up to $E_x \sim 2$ MeV are included: $3/2^+_{\mathrm{g.s.}}$, $5/2^+$, $7/2^+$, and $1/2^+$ states for ^{23}Na and $5/2^+_{\mathrm{g.s.}}$, $1/2^+$, $3/2^+$, $7/2^+$, and $5/2^+_2$ states for ^{25}Mg and ^{27}Al. For β decay, all the initial states with excitation energy below $E_x \sim 1.5$ MeV are included: $5/2^+_{\mathrm{g.s.}}$ and $1/2^+$ states for ^{23}Ne; $5/2^+_{\mathrm{g.s.}}$, $3/2^+$, and $1/2^+$ states for ^{25}Na; and $1/2^+_{\mathrm{g.s.}}$ and $3/2^+$ states for ^{27}Mg. As for final states, we take states up to about $E_x = 10$ MeV.

III. β-TRANSITION RATES FOR URCA NUCLEAR PAIRS

We calculate the β-transition rates of URCA nuclear pairs, which are relevant for the evolution of 8–10$M_\odot$ stars. They are $A = 23$, 25, and 27 nuclear pairs. Our intention here is to discuss in detail the properties of β transitions of the URCA nuclear pairs. For star calculations, we consider here that the tables of Oda *et al.* [10] are enough for discussions of other β-reaction rates. After making sure of the importance of the detailed URCA table for URCA β-transition rates in actual star calculations, we identify suitable mesh points for all the β transitions of *sd*-shell nuclei and make a new table to be used for stellar evolution calculations with finer mesh points.

A. ^{23}Ne and ^{23}Na URCA pair

We calculated wave functions of ^{23}Ne and ^{23}Na using the *sd*-shell model of Wildenthal [5]. We take a few excited states of the parent nucleus to consider the temperature effect. The transition rates and the neutrino-energy-loss rate and the γ-energy-gain rate are calculated using the formula of Fuller *et al.* [7].

We show in Fig. 1(a) the β-decay rates of ^{23}Ne as a function of temperature at the density of $\log_{10} \rho Y_e = 8.8$, which is just below the density of the URCA process which will be discussed later. In Fig. 1(b) we show the electron-capture rates of ^{23}Na as a function of temperature at the density of $\log_{10} \rho Y_e = 9.0$, which is just above the URCA density of the $A = 23$ nuclear pair. Here Y_e is the electron mole number and ρ is the nucleon density in units of g cm^{-3}. In both figures, two curves are shown, where the dashed curve is obtained including only the ground-state to ground-state transition and the solid curve is obtained including all the transitions. The

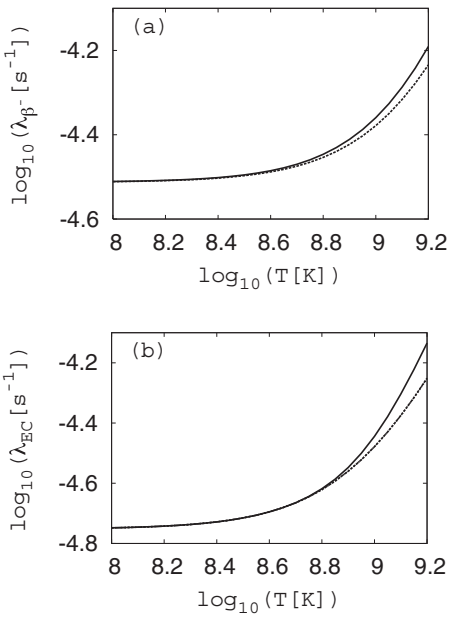

FIG. 1. β-decay rates of ^{23}Ne at the density of $\log_{10} \rho Y_e = 8.8$ (a) and electron-capture rates of ^{23}Na at the density of $\log_{10} \rho Y_e = 9$ (b) as a function of temperature in units of K. The dashed curves denote the β-transition rates of ground-state to ground-state transition, while the solid curves denote those of all the possible transitions.

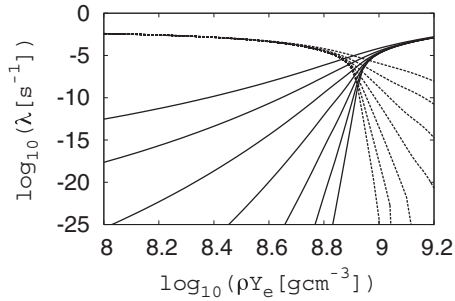

FIG. 2. β-transition rates for the $A = 23$ URCA nuclear pair (^{23}Ne, ^{23}Na) for various temperatures as functions of density $\log_{10} \rho Y_e$. β-decay rates (dashed lines) are those decreasing with density, while electron-capture rates (solid lines) are those increasing with density. The temperature steps are shown in the range of $\log_{10} T = 8$ to 9.2 in steps of 0.2.

effect of excited states in this temperature range is not large and becomes appreciable only above $\log_{10} T \sim 8.8$, where the second excited state of the parent nucleus is slightly populated and makes a small contribution to the reaction rates. Here T is the temperature in units of K.

We show calculated results of β-transition rates for the $A = 23$ URCA nuclear pair in Fig. 2. β-decay rates are shown for various temperatures in the range of $\log_{10} T = 8$ to 9.2 in steps of 0.2 as functions of density from $\log_{10} \rho Y_e = 8$ to 9.2. It is clearly seen that the β-decay rate becomes smaller as the density increases, while the electron-capture rate becomes larger as the density increases. At around $\log_{10} \rho Y_e = 8.92$, both the reaction rates are significantly large; this is the density range where the nuclear URCA process of the $A = 23$ pair takes place and the star is very effectively cooled down by the emission of both neutrinos and antineutrinos without changing the nuclear configurations and the electron abundance.

We want to discuss the effect of mesh points by showing the product of the two reaction rates in Fig. 3, because for the URCA process both the reaction rates have to be significantly large. In Fig. 3(a), the fine mesh points are used and the product is quite smooth even for the lowest temperature: $\log_{10} T = 8$. It is clearly seen that the peak position is at $\log_{10} \rho Y_e = 8.92$ and stays there as the temperature drops toward the lowest temperature shown here. On the other hand, the crude mesh points of $\Delta \log_{10} \rho Y_e = 1$, shown in Fig. 3(b), miss the peak of the product of the URCA process for the $A = 23$ pair. This is the case of the table of Oda *et al.* [10].

In order to see the mesh point effect further, we show in Fig. 4 two cases, $\Delta \log_{10} \rho Y_e = 0.06$ and 0.2, for the product of β-transition rates. As can be seen even for $\Delta \log_{10} \rho Y_e = 0.06$ [Fig. 4(a)], the URCA density becomes unclear as compared to the case of $\Delta \log_{10} \rho Y_e = 0.02$ as shown in Fig. 3. From this comparison of different mesh points in density, we conclude that the finer mesh points of $\Delta \log_{10} \rho Y_e = 0.02$ are necessary to describe the nuclear URCA process in the evolution of massive stars.

B. ^{25}Na and ^{25}Mg URCA pair

We calculated nuclear structures of the next URCA pair, ^{25}Na and ^{25}Mg, using the *sd*-shell model [5]. We then

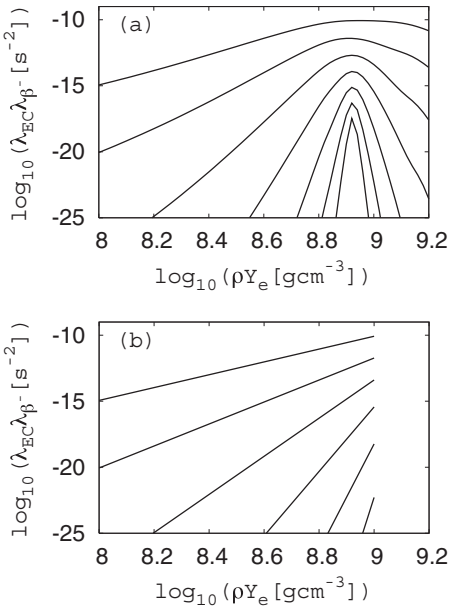

FIG. 3. Product of β-transition rates for the $A = 23$ URCA nuclear pair (^{23}Ne, ^{23}Na) for various temperatures as functions of density $\log_{10} \rho Y_e$. In panel (a), the mesh points are taken from $\log_{10} \rho Y_e = 8.0$ to 9.2 in steps of 0.02, while in panel (b), they are from $\log_{10} \rho Y_e = 8.0$ to 9.0 in a single step as in Oda *et al.* [10].

calculated β-transition rates using the formula of Fuller *et al.* [7]. We show first the role of excited states for these reaction rates in Fig. 5. In Fig. 5(a), we show the β-decay rate of ^{25}Na as a function of temperature at the density of $\log_{10} \rho Y_e = 8.6$, which is slightly below the URCA density for the $A = 25$ pair.

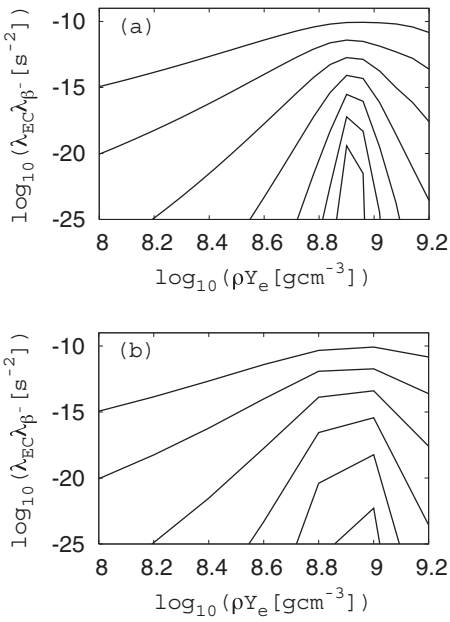

FIG. 4. Product of β-transition rates for the $A = 23$ URCA nuclear pair (^{23}Ne, ^{23}Na) for various temperatures as functions of density $\log_{10} \rho Y_e$. In panel (a), the mesh points are taken from $\log_{10} \rho Y_e = 8.0$ to 9.2 in steps of 0.06, while in panel (b), they are from $\log_{10} \rho Y_e = 8.0$ to 9.2 in steps of 0.2.

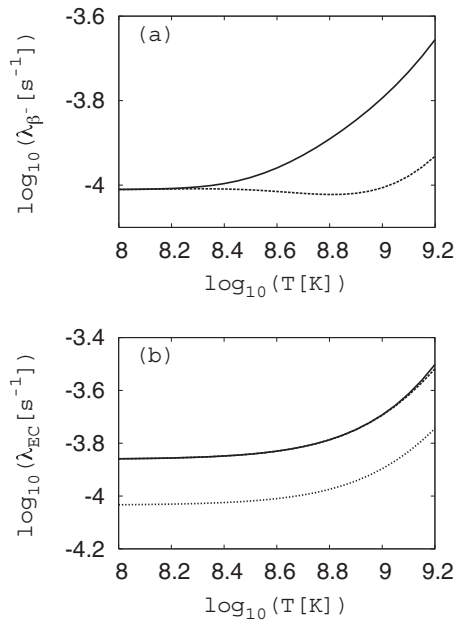

FIG. 5. β-decay rates of ^{25}Na at the density of $\log_{10} \rho Y_e = 8.6$ (a) and electron-capture rates of ^{25}Mg at the density of $\log_{10} \rho Y_e = 8.9$ (b) as functions of temperature. The dashed curves denote the β-transition rates of ground-state to ground-state transition, while the solid curves denote those of all the possible transitions. In panel (b), we also show the transition rates including the ground state to excited states by the dashed line, which are slightly below those shown by the solid line and seen only above $\log_{10} T = 9$.

Shown here by the dashed curve is the transition rate of the ground-state to ground-state transition. The transition rate of ground state to excited states is very small. The solid curve is for transition rates including all the excited states. The fact that the transition rate of the ground-state to ground-state transition (dashed curve) is reduced around $\log_{10} T = 8.8$ is related to the contribution of the excited states of the parent nucleus. The inclusion of excited states of the parent nucleus becomes significant starting at $\log_{10} T \sim 8.4$ and the population of the ground state of the parent nucleus is reduced following Eq. (4). In Fig. 5(b), we show electron-capture rate of ^{25}Mg as a function of temperature at the density of $\log_{10} \rho Y_e = 8.9$, which is slightly above the URCA density. The dashed curve denotes the ground-state to ground-state transition and the solid curve includes all the transitions. In this case, the contribution of the transition from the ground state to the excited states is important throughout the temperature range of interest. This fact is indicated by showing the ground-state to excited-state transitions by the dashed curve, which is only slightly smaller than the solid curve, and a tiny difference may be seen above $\log_{10} T = 9$.

We show the β-transition rates for the $A = 25$ URCA pair for various temperatures as functions of density in Fig. 6. As discussed above for the $A = 23$ URCA pair, the β decay decreases with density, while the electron capture increases with density. There is a density where both the reaction rates are significantly large and the URCA process takes place around $\log_{10} \rho Y_e = 8.78$.

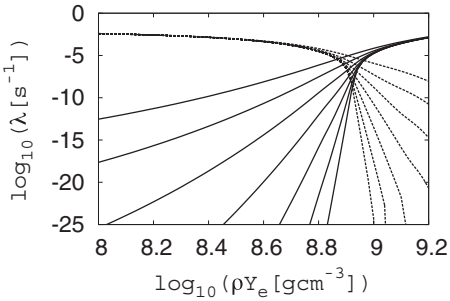

FIG. 6. β-transition rates for the $A = 25$ URCA nuclear pair (^{25}Na, ^{25}Mg) for various temperatures as functions of density $\log_{10} \rho Y_e$. β-decay rates are those decreasing with density, while electron-capture rates are those increasing with density. The temperature steps are shown in the range of $\log_{10} T = 8$ to 9.2 in steps of 0.2.

C. ^{27}Mg and ^{27}Al URCA pair

We calculated nuclear structures of a heavier URCA pair, ^{27}Mg and ^{27}Al, using the sd-shell model. We then calculated β-transition rates using the formula of transition rates. We discuss first contributions of excited states in β-transition rates. We point out that the ground-state to ground-state transition is zero, because the ground-state spin of ^{27}Mg is $1/2^+$ and the ground-state spin of ^{27}Al is $5/2^+$ and the GT matrix element is zero. We show in Fig. 7(a) β-decay rates of ^{27}Mg at $\log_{10} \rho Y_e = 8.28$ as a function of temperature. Here, the full strength includes contributions of excited states to excited states, which become significant above $\log_{10} T = 8.4$. We show in Fig. 7(b) electron-capture rates for ^{27}Al at $\log_{10} \rho Y_e = 8.5$ as a function of temperature. For this transition, excited states of the parent nucleus to final states become significant above $\log_{10} T = 8.6$.

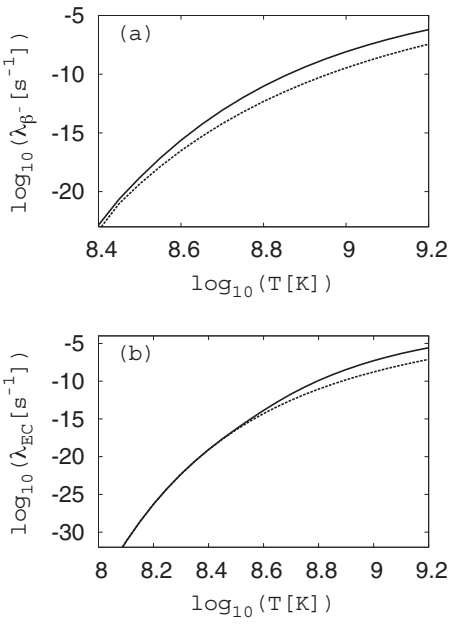

FIG. 7. β-decay rates of ^{27}Mg at the density of $\log_{10} \rho Y_e = 8.28$ (a) and electron-capture rates of ^{27}Al at the density of $\log_{10} \rho Y_e = 8.5$ (b) as functions of temperature $\log_{10} T$. The dashed curves denote the β-transition rates of ground state to excited states, while the solid curves denote those of all the possible transitions.

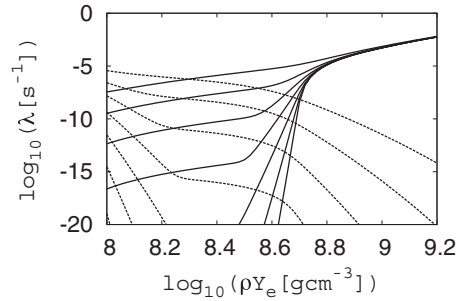

FIG. 8. β-transition rates for the $A = 27$ URCA nuclear pair (^{27}Mg, ^{27}Al) for various temperatures as functions of density $\log_{10} \rho Y_e$. β-decay rates are those decreasing with density, while electron-capture rates are those increasing with density. The temperature steps are shown in the range of $\log_{10} T = 8$ to 9.2 in steps of 0.2.

We show in Fig. 8 β-transition rates for the $A = 27$ URCA pair for various temperatures as functions of density. For this URCA pair, there is no sharp density where both β-transition and electron-capture rates are large enough. If we plot products of the β-transition rates for the $A = 27$ pair, the curve changes gradually with density and there is no peak as in the cases of the $A = 23$ and 25 pairs. This is related to the fact that the ground-state to ground-state transition is forbidden because the spin difference is 2 and the $M1$ transition is not allowed. Hence, the URCA process happens only gradually in a large density range. This fact leads to the URCA process happening successively from the $A = 25$ URCA process and then the $A = 23$ URCA process in stellar evolution, once the conditions for the density and temperature suited for the URCA process are met.

IV. COULOMB CORRECTIONS

It is important to include the Coulomb corrections to electron-capture rates of nuclei in the stellar evolution, where the electron Fermi energy is large and electron pressure supports massive stars [13,14]. For URCA β transitions in stars we should consider the Coulomb corrections not only for electron capture but also for β decay due to large Fermi energy. In the stellar environment of our concern, electrons are partially in the plasma phase. Those electrons are attracted by the Coulomb potential of a nucleus and influence β-transition rates. This Coulomb effect was worked out in detail by Itoh *et al.* [14]. We follow their method for the inclusion of the Coulomb corrections for both the electron capture and the β decay of the URCA pairs.

We write several steps to obtain the formula for the Coulomb corrections to electron-capture and β-decay rates. The Coulomb potential $-\frac{Ze^2}{r}$ should be replaced by $V(r)$ including screening effects of relativistically degenerate electron liquid. We are able to include the screening effect by calculating the dielectric function $\epsilon(q, 0)$ using the relativistic random phase approximation [14]. Hence, we can get a screened

Coulomb potential by defining its Fourier transformation as

$$V(r) = -\frac{Ze^2}{2\pi^2}\int \frac{e^{i\vec{k}\vec{r}}}{k^2\epsilon(k,0)}d^3k = -\frac{Ze^2 2k_F}{2k_F r}\frac{2}{\pi}\int \frac{\sin(2k_F qr)}{q^2\epsilon(q,0)}dq. \quad (8)$$

We define the increment potential due to screening effect as

$$V_s(r) = V(r) - \left(-\frac{Ze^2}{r}\right) = Ze^2(2k_F)J, \quad (9)$$

where

$$J = \frac{1}{2k_F r}\left(1 - \frac{2}{\pi}\int \frac{\sin(2k_F qr)}{q^2\epsilon(q,0)}dq\right). \quad (10)$$

This screening coefficient J is tabulated in the paper of Itoh *et al.* [14]. With this correction factor, we calculate

$$f_{ij}^C = f_{ij}[T, \rho_e, U_F - V_S(0)]. \quad (11)$$

Because $V_S(0)$ is a small positive value as compared with the chemical potential U_F, the Coulomb correction effect is to reduce both electron-capture and β-decay rates.

Another effect due to the Coulomb corrections is the change of the threshold energy,

$$\Delta Q_C = \mu_C(Z-1) - \mu_C(Z), \quad (12)$$

where $\mu_C(Z)$ is the correction of the chemical potential of the nucleus with charge number Z due to the interactions of the nucleus with the electron background [13,15,16]. The Coulomb chemical potential of a nucleus with Z in a plasma of density ρ, electron number density n_e, and temperature T is given by

$$\mu_C(Z) = kTf(\Gamma), \quad (13)$$

with $\Gamma = Z^{5/3}\Gamma_e$, $\Gamma_e = \frac{e^2}{kTa_e}$, and $a_e = (\frac{3}{4\pi n_e})^{1/3}$. The function f for $\Gamma > 1$ is given as [17]

$$f(\Gamma) = a\Gamma + 4b\Gamma^{1/4} - 4c\Gamma^{-1/4} + d\ln\Gamma + e, \quad (14)$$

with $a = -0.898\,004$, $b = 0.967\,86$, $c = 0.220\,703$, $d = -0.860\,97$, and $e = -2.526\,92$, while for $\Gamma < 1$ it is expressed as

$$f(\Gamma) = -\frac{1}{\sqrt{3}}\Gamma^{3/2} + \frac{\beta}{\gamma}\Gamma^{\gamma}, \quad (15)$$

with $\beta = 0.295\,614$ and $\gamma = 1.988\,48$, which are determined by requiring the continuity of f and $\frac{df}{d\Gamma}$ at $\Gamma = 1$.

As $\mu_C(Z)$ is negative, the energy threshold increases with the screening effects, and the capture rates are reduced. In case of the inverse β transition, the increase of the Q value leads to the enhancement of the phase space, and the β-decay rates are increased. We show in Fig. 9 calculated electron-capture and β-decay rates for mass $A = 25$ with the screening effects as well as those without the screening effects.

The screening effects are found to change the rates by several times or more at certain ranges of $\log_{10}\rho Y_e$. Dominant contributions of the screening effects come from the change of the Coulomb chemical potential $\mu_C(Z)$ of the nuclei. The screening effects on the electron energy are very small in the present density and temperature region. Hence, if we shift the density by a small amount corresponding to the shift of the value of the chemical potential at the threshold, we find that this shift simulates the screening effects fairly well for both the electron-capture and β-decay rates. This corresponds to the change of the density by $\Delta\log_{10}\rho Y_e = 0.04$. It would be quite interesting to study the screening effects on the URCA processes.

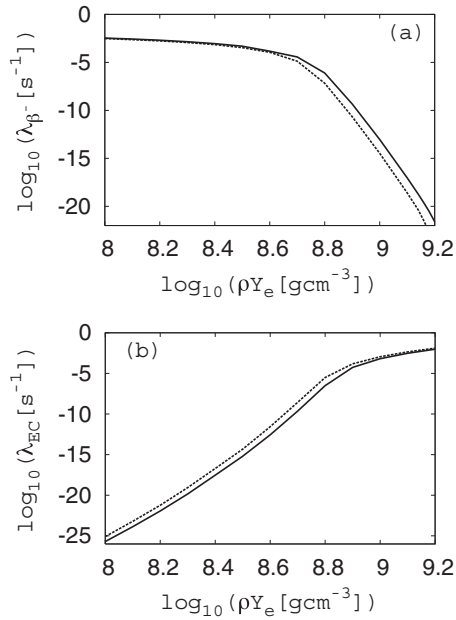

FIG. 9. Coulomb screening effects on β-decay rates for ^{25}Na $\rightarrow$ ^{25}Mg (a) and electron-capture rates for ^{25}Mg $\rightarrow$ ^{25}Na (b) as functions of density at $\log_{10} T = 8.7$. The solid curves are those with the Coulomb correction and the dashed curves are those without the Coulomb correction.

V. EFFECTS ON STELLAR EVOLUTION

It is very interesting to see effects of the new table of the β-transition rates of the URCA nuclear pairs on stellar evolution. We show here one example of stellar evolution calculations where the effect of the URCA cooling is clearly seen [18]. The results are shown in Fig. 10 for the time evolution of the central temperature in the $8.8M_\odot$ star. This star forms an electron-degenerate O-Ne-Mg core after C burning in the central region and, during $t = 0$ to 4 yr in Fig. 10, its central density increases from $\log_{10}\rho = 9.0$ to 9.4. We have used two URCA reaction tables. One table is obtained with the fine mesh points of the present study. The other is Oda *et al.*'s table [10], where very scarce mesh points are used. These two tables for β-transition rates are compared in Fig. 3. We see two distinct drops of the temperature due to $A = 25$ URCA cooling up to around $t = 1$ yr and due to $A = 23$ URCA cooling between $t = 2$ yr and $t = 2.5$ yr. When the temperature drops take place, the abundances of ^{25}Mg and ^{23}Na also drop due to the electron captures eventually dominating over β decays, respectively. Such a distinct temperature drop is not seen for the case of Oda *et al.*'s table [10]. The sharp drops around $t = 3$ yr and $t = 3.7$ yr are due to sudden expansion caused by neon shell flash in the outer layers. As a result

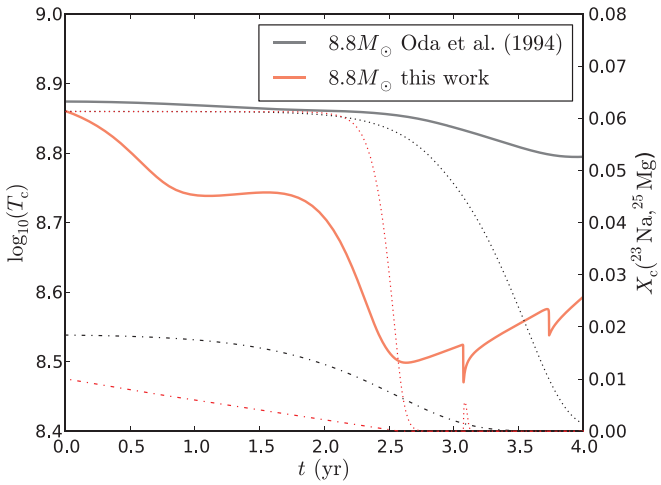

FIG. 10. (Color online) The evolution of the central temperature T_c of the $8.8M_\odot$ star as a function of time in units of years. The star forms an O-Ne-Mg core and, during $t = 0$ to 4 yr, its central density increases from $\log_{10}\rho = 9.0$ to 9.4. The temperature drop up to around $t = 1$ year is caused by the $A = 25$ URCA process and the temperature drop between $t = 2$ yr and $t = 2.5$ yr is caused by the $A = 23$ URCA process. Shown also are the time changes of the amounts of ^{25}Mg and ^{23}Na, and the mass fraction X_c of these nuclei decreases quickly in the place of the temperature drop due to the $A = 25$ and $A = 23$ URCA processes, respectively. We show also the case of Oda *et al.*'s table [10], where there is no effect of the URCA process. The URCA processes are completely missed when using this sparse grid.

of the large temperature drop due to URCA cooling, it is clear that the $8.8M_\odot$ star is undergoing collapse triggered by subsequent electron capture on ^{24}Mg and ^{20}Ne [4] rather than thermonuclear explosion triggered by Ne and O burning.

VI. SUMMARY

We have studied β-transition rates of URCA nuclear pairs expected to have impacts on the evolution of 8–$10M_\odot$ stars. They are the nuclear URCA pairs with masses of $A = 23$, 25, and 27. We took fine mesh points in temperature and density. This fine mesh is able to provide clearly the URCA density at $\log_{10}\rho Y_e = 8.92$ for $A = 23$ and at $\log_{10}\rho Y_e = 8.81$ for $A = 25$, while the URCA density is not clear for $A = 27$. We have discussed the effect of the Coulomb corrections on the β-transition rates. The screening effects have been found to change the rates by several times or more at a certain range of $\log_{10}\rho Y_e$. We have applied the new reaction rates for the evolution of the $8.8M_\odot$ star. The two tables, ours and Oda *et al.*'s table [10], provide quite different temperature evolutions in the central region. The new table clearly shows the effect of the nuclear URCA process to decrease the core temperature, while Oda *et al.*'s table [10] completely misses the URCA cooling process in the evolution of the star.

We prepared a table for the β-reaction rates and neutrino-energy-loss rates and γ-energy-heating rates for the URCA nuclear pairs, $A = 23$, 25, and 27, in the range of density $8.0 < \log_{10}\rho Y_e < 9.2$ in steps of 0.02 and temperature $8.0 < \log_{10} T < 9.2$ in steps of 0.05. We made the data file of these reaction rates together with the neutrino-energy-loss rates and the γ-energy-gain rates for the use of stellar evolution calculations, which are available upon request.

ACKNOWLEDGMENTS

We are grateful to Professor A. Brown for providing us with the ft values of the URCA nuclear pairs in the early stage of this work. This work has been supported in part by Grants-in-Aid for Scientific Research No. (S)23224004, No. (S)21540267, No. (C)23540262, and No. (C)22540290 and the World Premier International Research Center Initiative of the MEXT of Japan. R.H. and S.J. acknowledge support from the European Research Council under the European Union's Seventh Framework Programme (FP/2007-2013)/ERC Grant Agreement No. 306901. R.H. and S.J. also acknowledge support from the ESF EUROCORES programme EuroGENESIS.

[1] K. Nomoto and M. Hashimoto, Phys. Rep. **163**, 13 (1988).
[2] S. Miyaji, K. Nomoto, K. Yokoi, and D. Sugimoto, Pub. Astron. Soc. Jpn. **32**, 303 (1980).
[3] K. Nomoto, Astrophys. J. **277**, 791 (1984).
[4] K. Nomoto, Astrophys. J. **322**, 206 (1987).
[5] B. H. Wildenthal, Prog. Part. Nucl. Phys. **11**, 5 (1984).
[6] B. A. Brown and B. H. Wildenthal, Phys. Rev. C **28**, 2397 (1983); Nucl. Phys. A **474**, 290 (1987); Ann. Rev. Nucl. Part. Sci. **38**, 29 (1988).
[7] G. M. Fuller, W. A. Fowler, and M. J. Newman, Astrophys. J., Suppl. Ser. **42**, 447 (1980).
[8] T. Kajino, E. Shiino, H. Toki, B. A. Brown, and B. H. Wildenthal, Nucl. Phys. A **480**, 175 (1988).
[9] M. Takahara, M. Hino, T. Oda, K. Muto, A. A. Wolters, P. W. M. Glaudemans, and K. Sato, Nucl. Phys. A **504**, 167 (1989).
[10] T. Oda, M. Hino, K. Muto, M. Takahara, and K. Sato, At. Data Nucl. Data Tables **56**, 231 (1994).
[11] B. A. Brown and B. H. Wildenthal, At. Data Nucl. Data Tables **33**, 347 (1985).
[12] B. A. Brown and W. A. Richter, Phys. Rev. C **74**, 034315 (2006); W. A. Richter, S. Mkhize, and B. A. Brown, *ibid.* **78**, 064302 (2008).
[13] A. Juodagalvis, K. Langanke, W. R. Hix, G. Martinez-Pinedo, and J. M. Sampaio, Nucl. Phys. A **848**, 454 (2010).
[14] N. Itoh, N. Tomizawa, M. Tamamura, and S. Wanajo, Astrophys. J. **579**, 380 (2002).
[15] W. L. Slattery, G. D. Doolen, and H. E. DeWitt, Phys. Rev. A **26**, 2255 (1982).
[16] R. Mochkovitch and K. Nomoto, Astron. Astrophys. **154**, 115 (1986).
[17] S. Ichimaru, Rev. Mod. Phys. **65**, 255 (1993).
[18] S. Jones, R. Hirschi, K. Nomoto, T. Fischer, F. X. Timmes, F. Herwig, B. Paxton, H. Toki, T. Suzuki, G. Martinez-Pinedo, Y. H. Lam, and M. Bertolli, arXiv:1306.2030 [Astrophys. J. (to be published)].